Defect-strain engineering for multiferroic and magnetoelectric properties in epitaxial (110) ferroelectric lead titanate

Tao Xu,[1,*] Takahiro Shimada,[1,†] Yasumitsu Araki,[1] Jie Wang,[2] and Takayuki Kitamura[1]
[1]*Department of Mechanical Engineering and Science, Kyoto University, Nishikyo-ku, Kyoto 615-8540, Japan*
[2]*Department of Engineering Mechanics, School of Aeronautics and Astronautics, Zhejiang University, Hangzhou 310027, China*
(Received 7 April 2015; revised manuscript received 15 July 2015; published 14 September 2015)

The quest for multiferroics with coexisting ferroic orders, such as ferroelectricity and (anti-)ferromagnetism, in a single phase continues to arouse interest by the promise of novel functions and technological device paradigms. However, the mutually exclusive mechanism of ferroelectricity and magnetism has limited the discovery and understanding of novel multiferroic materials. Here we demonstrate using the hybrid functional of Hartree-Fock and density-functional theories that an unusual interaction between oxygen vacancies and misfit (epitaxial) strains brings about local magnetic moments with different orders coexisting with the host ferroelectricity of nonmagnetic (NM) $PbTiO_3$ due to orbital symmetry breaking of the defect electronic states. The emerging magnetic spin moment exhibits rich local order transitions in response to switching the spontaneous polarization, i.e., magnetoelectric coupling. Individual oxygen vacancies therefore act as a source of ferroic-order parameters. The multiferroic and magnetoelectric properties exploited by engineering defects and strains provide an alternative route for multiferroics and will open a new avenue for multifunctional oxides that exhibit magnetism coexisting with host functionalities.

DOI: 10.1103/PhysRevB.92.104106 PACS number(s): 77.80.−e, 75.85.+t, 61.72.jd, 31.15.E−

I. INTRODUCTION

In recent years, multiferroic materials with coexisting magnetic and ferroelectric ordering in the same phase have attracted considerable attention owing to their new physical properties and potential applications [1,2]. The strong cross coupling between the ferroelectric and ferromagnetic orders in multiferroic materials, i.e., the magnetoelectric (ME) effect, allows the magnetic field manipulation of ferroelectric or, conversely, electric field control of magnetic properties, which holds promise for advanced technological devices, such as magnetoelectric sensors, multiple-state memories, and multifunctional photonic devices [3–5]. Considerable efforts have been devoted to fabricating multiferroic materials, including single-phase materials [6,7] and multiphase composites combining ferroelectric and ferromagnetic phases [8,9]. Nevertheless, the understanding and discovery of new high-performance multiferroics remain limited. Perovskite-based ferroelectric materials are excellent candidates for potential multiferroic materials because of their excellent piezoelectric response and particularly large spontaneous polarization. However, such traditional ferroelectric materials, including $PbTiO_3$ and $BaTiO_3$, are intrinsically nonmagnetic because the d^0 electronic configuration of the transition metal Ti^{4+} ions in these ferroelectric materials clearly contradicts a requirement of magnetism, namely, the partial occupation of d states [10].

Oxygen vacancies, one of the most abundant types of defects in oxide materials, are inherently present in ferroelectric oxide thin films during their synthesis and deposition processes [11]. The presence of these vacancies not only gives rise to a partial loss of short-range interactions, but also breaks the balance of long-range Coulombic interactions when positively or negatively charged. Thus, ferroelectricity, which originates from a delicate balance between long-range Coulombic interactions and short-range repulsive interactions, can be strongly affected by oxygen vacancies. Moreover, oxygen vacancies can bring about an intriguingly rich variety of additional phenomena and functionalities that perfect host materials do not possess, such as n-type conductivity [12], unexpected dielectric response around room temperature [13], etc. However, oxygen vacancies have nothing to do with the desired multiferroics because of the spin unpolarized nature of the defect states, as verified by the hybrid Hartree-Fock density functional [14]. Therefore, an alternative design concept and route for multiferroic materials with nonmagnetic ferroelectrics is necessary, rather than merely the introduction of vacancies. On the other hand, ferroelectric thin films are normally fabricated by epitaxial growth on thick substrates, unavoidably resulting in tensile or compressive strains. Epitaxial strain plays an important role in tuning ferroelectric, magnetoelectric, and other properties [15–18]. Generally, strain and defects are intrinsically coupled: vacancies can induce local perturbation of the lattice and generate tensile and compressive stresses, while strains can tune the vacancy configuration and formation energy [19,20]. With these two key ingredients of the modification of material properties intertwined and indispensable in ferroelectric oxide perovskite, a sound fundamental understanding of their interaction and driven properties would be crucial for materials design and of scientific interest. Particularly, the (110) misfit strain is fundamentally different from the common (001) strain, which makes it possible to break lattice symmetry and hence obtain new crystal phases and novel functionalities that are not available in the case of the (001) strain [21,22].

In this study we present a path toward the realization of multiferroic properties in oxygen-deficient epitaxial (110) ferroelectrics based on the convincing hybrid Hartree-Fock density-functional theories. The $PbTiO_3$ phase diagram is obtained as a function of the (110) epitaxial strain. Importantly, it is successfully determined that oxygen vacancies in

*xu.tao.44a@st.kyoto-u.ac.jp
†shimada@me.kyoto-u.ac.jp

combinations with the (110)-oriented misfit strain give rise to local magnetic moments with different orders, depending on the symmetry breaking of the vacancies. The origin of the moments and the physics behind their appearance are revealed from the electronic structures. Furthermore, we suggest the existence of a nonlinear magnetoelectric (ME) effect through the switching of the ferroelectric polarization.

II. COMPUTATIONAL DETAILS

A. Simulation method

First-principles calculations based on density-functional theory (DFT) are performed with the VASP program code [23,24], using the projector-augmented wave potentials [25] that explicitly treat the Pb $5d$, $6s$, and $6p$, the Ti $3s$, $3p$, $3d$, and $4s$, and the O $2s$ and $2p$ electrons as valence states. A plane-wave basis set with an energy cutoff of 500 eV is chosen for the electronic wave function. $2 \times 2 \times 2$ Monkhorst-Pack k-point mesh [26] is used for Brillouin zone (BZ) integrations. The effect of spin polarization is included in all calculations. The Heyd-Scuseria-Ernzerhof (HSE06) screened hybrid functional [27,28] is employed as the exchange, which incorporates 25% of the exact exchange from Hartree-Fock theory and 75% exchange from the Perdew-Burke-Ernzerhof functional (PBE) [29] of the generalized gradient approximation (GGA), as suggested by Heyd *et al.* [27]. A screen parameter of 0.2 Å^{-1} is used for the semilocal exchange as well as for the screened nonlocal exchange. The commonly used local or semilocal approximations of DFT, such as local density approximation (LDA) or GGA yield significantly underestimated band gaps [30,31], which can pose serious problems in the description of energy, defect electronic structures, and other defect-related properties. The severe underestimation of the band gaps leads, for instance, to the incorrect capture of the defect state in the vicinity of the conduction band minimum (CBM) rather than within the band gap, which cannot reflect the true physics of the defect state. The HSE06 hybrid functional, on the other hand, has been tested for various wide-band-gap oxides and proved to be rationale and essential for the reproduction of not only the lattice constant and elastic properties but also band gaps with extremely high accuracy for various insulators and semiconductors [14,32]. The tetragonal lattice constant obtained from the HSE06 hybrid functional used for bulk ferroelectric $PbTiO_3$ is $a = 3.86$ Å ($c/a = 1.071$) and the band gap is $E_{gap} = 3.4$ eV. Both of these values are in fairly good agreement with experimental data of $a = 3.88$Å, $c/a = 1.071$, and $E_{gap} = 3.4$ eV, respectively [33,34], indicating the viability and effectiveness of the functional in describing the structural and electronic properties of the oxygen vacancy in the perovskite ferroelectric oxide $PbTiO_3$.

B. Simulation models and procedure

Figure 1(a) illustrates the simulation supercell constructed from the prototype unite cell with the spontaneous polarization along [100]. The x, y, and z axes in the Cartesian setting are along [1$\bar{1}$0], [001], and [110] directions, respectively. The supercell contains 120 atoms and the dimensions in the x, y, and z directions are $2\sqrt{2}a_{sub}$, $3a_{sub}$, and $2\sqrt{a^2+c^2}$,

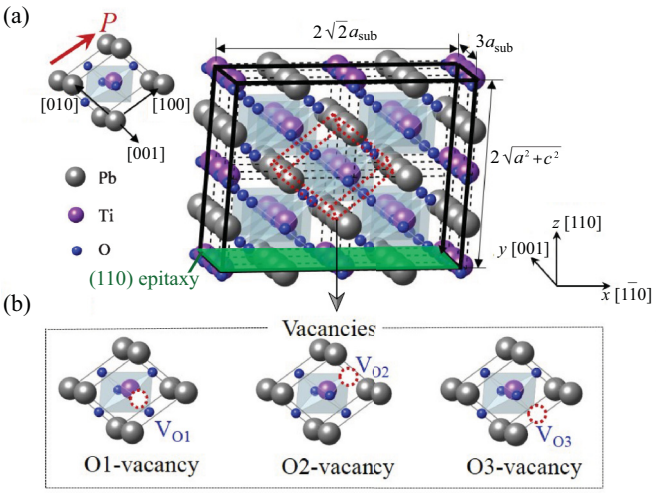

FIG. 1. (Color online) Simulation model for O1, O2, and O3 vacancies in (110) epitaxial $PbTiO_3$. (a) The simulation supercell model for (110) epitaxial $PbTiO_3$ used in the present study. The supercell contains 120 atoms. The green plane shows the epitaxial (110) plane subjected to misfit strain. (b) Three different kinds of oxygen vacancies in the model, V_{O1}, V_{O2}, and V_{O3}.

respectively, where a_{sub} is the cubic lattice parameter of the (110) substrate, and a and c are the lattice constants of tetragonal $PbTiO_3$ obtained from the HSE06 hybrid functional. To study the effect of (110) epitaxial strain, we use the bulk supercell with the periodic boundary condition under (110) pseudoepitaxy, which does not include the effect of (110) surface that is considered in a previous study [35]. The epitaxial constraint from (110)-oriented cubic substrates with different lattice parameters (a_{sub}) is treated implicitly by constraining the in-plane vectors of the supercell. The lowest energy structure of the supercell with a substrate lattice parameter $a_{sub} = a_\circ$ is set as the zero misfit strain state under such (110) pseudoepitaxy condition. Hence, the misfit strain is defined as $\varepsilon = (a_{sub} - a_\circ)/a_\circ$ and a range of in-plane misfit strains from -4% to $+4\%$ are considered in the following. During the calculations, the two in-plane vectors are kept fixed to simulate the (110) pseudoepitaxy, while the out-of-plane vector and internal atomic positions are fully relaxed until the maximum Hellmann-Feynman forces are less than 0.01 eV/Å.

An oxygen vacancy inside $PbTiO_3$ films, denoted as $V_i (i = O1, O2, O3)$, is simulated by removing the corresponding oxygen atom from the calculated supercell and then relaxing the atomic positions at each epitaxial condition. Owing to the symmetry breaking of the supercell under epitaxial (110) strain, there are three kinds of inequivalent oxygen vacancies in the model that are located in the nonpolar [001] and [010] directions (V_{O1}, V_{O3}), and the polar [100] direction (V_{O2}) relative to the Ti atom, respectively [see Fig. 1(b)]. Note that O1 and O3 are also nonequivalent with Ti-O-Ti chains lying in and out of the strained (110) plane, respectively. Therefore, Ti-O1-Ti chains and Ti-O3-Ti chains suffer from different strain fields and can lead to different atomic displacement. Specifically, as the increasing of compressive misfit strains, the polarization in [010] will gradually increase due to the lattice elongation in this direction and O3 atoms will move

along this direction, while the in-plane polarization remains zero and the central symmetry of Ti-O1-Ti bonds are retained. These differences are closely related to the magnetic properties of oxygen vacancies, as will be discussed later.

III. RESULTS

A. Crystal phase stabilities under different misfit strains

For the present range of epitaxial strains, the epitaxial (110) $PbTiO_3$ exhibits three types of low-symmetry ferroelectric phases according to their geometrical character (α, β, and γ), viz., the monoclinic $M_C(Pm;\beta=\gamma=90^\circ,\alpha\neq 90^\circ)$, orthorhombic $O(Amm2;\beta=\gamma=\alpha=90^\circ)$, and triclinic Tri($P1;\beta\neq\alpha\neq\gamma=90^\circ$) phases. Here γ denotes the angle between two in-plane cell vectors, which is always fixed to be 90° due to the epitaxial constraint, and α and β are the angles between the out-plane cell vector and two in-plane cell vectors, respectively, as illustrated in Fig. 2. To determine the strain dependence of the equilibrium crystal structure, total energy optimization of the epitaxial (110) structure in these three crystal phases with various lattice parameter a_{sub} are performed separately. The total energy and spontaneous polarization as a function of misfit strain ε is calculated as shown in Fig. 2. The polarization is calculated by the modern theory of polarization based on the Berry phase theory. The lowest energy structure is the M_C phase, characterized by a combined polarization along the x and z directions (roughly the [100] direction) at zero misfit strain ($a_{sub}=3.94$ Å). It should be pointed out that the pseudoepitaxy of the $PbTiO_3$ on such an optimal (110) substrate, which is defined as zero-strain state, is actually under nonzero stress state and different from the "free-standing" unstrained system. With increasing tensile strain, the total energy of the M_C phase increases, triggering a transition to the triclinic phase at a critical misfit strain of 0.5%. In this phase, a polarization component appears along the y direction, and the direction turns to nearly $50\bar{1}$] at this critical point. Then, the total energy increases with increasing tensile strain. At the same time, the in-plane polarization component (x and y directions) tends to increase as well, whereas the out-of-plane polarization component (z direction) decreases, indicating that the polarization gradually rotates to [$1\bar{1}\bar{1}$], as shown in Fig. 2. The total energy of the M_C phase also increases with increasing compressive strain, and the polarization gradually rotates from [100] to [110] as its component along the z direction increases while that along the x direction decreases. This trend continues until the compressive strain exceeds 1.8%, at which point the M_C phase becomes metastable, in favor of the O phase with its polarization lying along the purely out-of-plane [110] direction (M_C-O phase transition). In the following study we focus on the phases that have the lowest total energy for each in-plane strain.

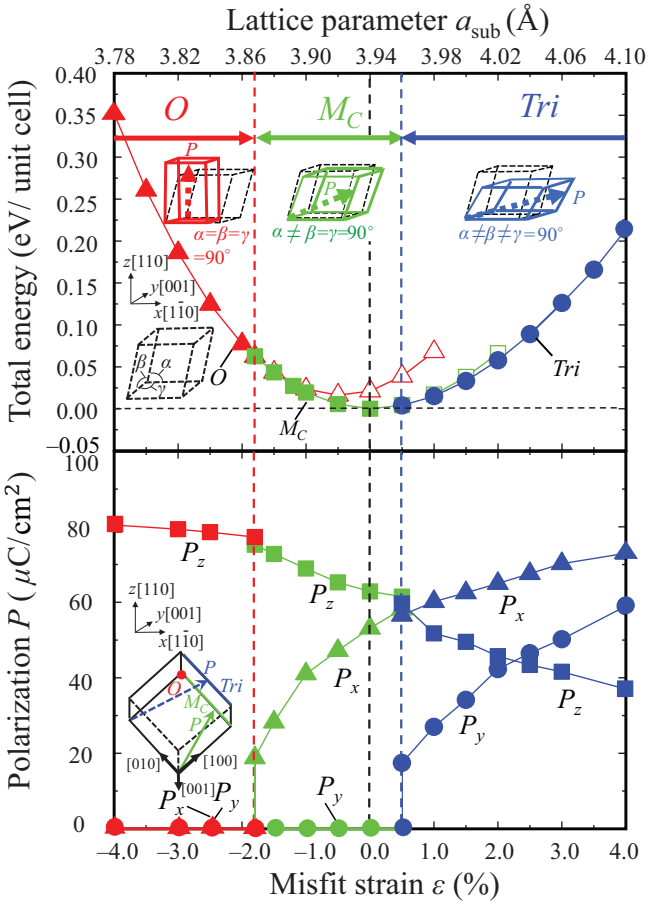

FIG. 2. (Color online) Crystal phase diagrams and the corresponding spontaneous polarization in epitaxial (110) $PbTiO_3$. The red and blue dotted lines indicate the M_C-O and M_C-Tri phase transitions, respectively. The dotted line structure on the top of the figure denotes the lowest energy structure. The P_x, P_y, and P_z correspond to polarization along [110], [001], and [110] directions, respectively.

B. Magnetic moments and defect electronic structures

The magnetic properties of three oxygen vacancies in epitaxial (110) $PbTiO_3$ are calculated (see Fig. S1 in Supplemental Material Ref. [36]). All the magnetic phases have a magnetic moment of $2.0\mu_B$ which is insensitive to the magnitude of strain. For the strain-free state of M_C phase, no spin moment is observed in any of the three types of oxygen vacancies, in agreement with the previous results of hybrid function studies on oxygen vacancies in strain-free ferroelectric oxides [14]. On the other hand, when the misfit strain is larger than 1.5% (as in the triclinic phase), magnetic moment emerges in V_{O1}. As seen in Fig. 3(a), the emerged magnetic moment is positive and mainly concentrated around the neighboring Ti atom located in the [001] direction with respect to the V_{O1} site. To shed further light on the origin of this magnetic moment in oxygen-deficient epitaxial (110) $PbTiO_3$, the electronic density of states (DOS) of V_{O1} are analyzed comprehensively. In fairly good agreement with previous studies [14], for V_{O1} in the strain-free thin film [see Figs. S2(a) and S2(b) in Supplemental Material Ref. [36]], the defect state is fully occupied by an up and down spin within the band gap, thus resulting in the nonmagnetic (NM) character of V_{O1}. The spatial distribution of squared wave function $|\psi_e|^2$ of the defect state, which is evaluated by using the energy range of the defect state in DOS, reveals that the defect state is a d_{z^2} orbital localized around the two adjacent Ti atoms. By contrast, for the V_{O1} in the triclinic phase at $\varepsilon=3.0\%$ [see Fig. 3(b)], we can find two distinct localized in-gap defect states, which are located at levels of 1.44 and 1.85

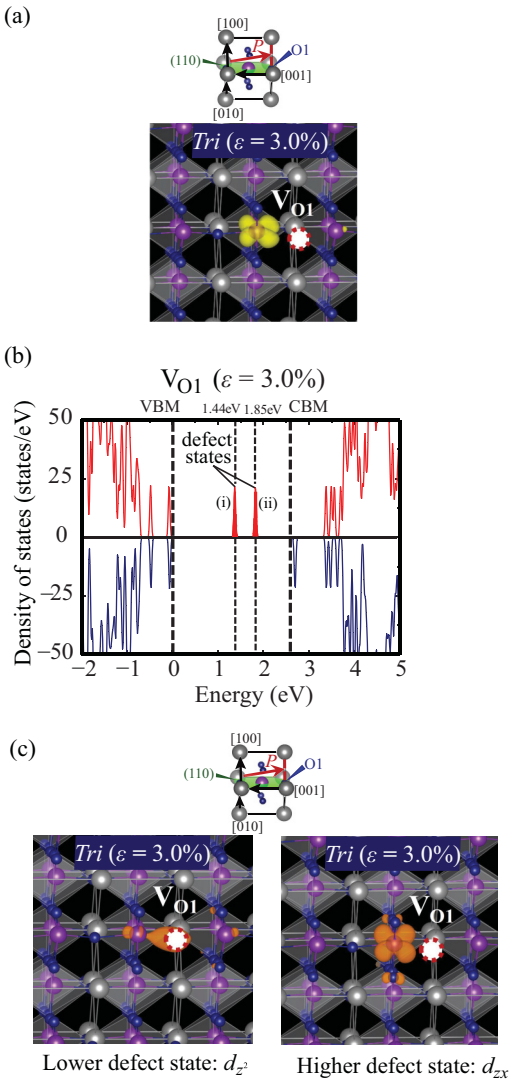

FIG. 3. (Color online) Spatial magnetization density distribution and defect electronic structures of V_{O1}. (a) Spatial magnetic spin-density distribution around V_{O1} in the triclinic phase. (b) Electronic density of states (DOS) of magnetic V_{O1}. Red and blue indicate the majority and minority spin states, respectively. (c) Squared wave functions of defect states in the triclinic phase. The original d_{z^2} defect state break into lower-level d_{z^2} and higher-level d_{zx} states in this phase. The orange and light blue iso-surfaces are the majority and minority spin densities of 0.015 $Å^{-3}$, respectively.

eV above the valence band maximum (VBM), respectively. Interestingly, both of these defect states are now partially occupied by a spin-up electron, and thus are spin polarized. This spin polarization of the defect states is responsible for the local magnetic moment that emerges in V_{O1}. Inspection of the shapes of the squared wave functions in Fig. 3(c) reveals that the lower defect state is localized at the adjacent Ti atom possessing a d_{z^2} orbital character, which is identical to that of the V_{O1} in the strain-free state, while the higher defect state is dominated by a new distinctive d_{zx} orbital. The appearance of this new d_{zx} defect state leads to splitting of the original fully occupied state into two partially occupied states. This crucial d_{zx}-dominated defect state may arise from the symmetry breaking of the triclinic phase through (110) tensile epitaxial strain: In the strain-free M_C phase, the crystal structure nearly close to tetragonal $P4mm$ symmetry with spontaneous polarization along the [100] direction. The application of a tensile misfit strain breaks the mirror symmetry in the [001] and [010] directions as the polar axis gradually rotates toward these two directions, resulting in two nonequivalent Ti atoms adjacent to the vacancy. Thus, the crystal phase transition to a lower symmetry breaks the orbital symmetry of the initial d_{z^2}-dominant defect state, and at the same time, induces the additional d_{zx}-dominant state.

As in the case of V_{O1}, a nonzero spin moment is also observed for the V_{O2} configuration in the tensile-strained structure [see Fig. 4(a)], whereas the critical point for the emergence of magnetic moment is located at a strain of 0.5%, where the M_C-Tri phase transition occurs. Moreover, a nonzero spin moment is also found when V_{O2} forms in the O phase under compressive strains larger than 1.8%, where no magnetic moment is observed in the former, V_{O1} case. Such spin moment observed in V_{O2} under misfit strains can be traced to a similar origin.V_{O2} without misfit strain does not induce splitting of the up-spin and down-spin defect states either, with two electrons occupied in the defect state. This defect state exhibits a localized feature in the vicinity of V_{O2} and the neighboring Ti atom, characterized by a $d_{x^2-y^2}$ orbital, as seen in Figs. S2(c) and S2(d) in Supplemental Material Ref. [36]. In contrast, we observe orbital symmetry breaking of the defect electronic structures of V_{O2} in both the O and Tri phases. For V_{O2} in the triclinic phase, a new occupied localized state is created owing to the symmetry breaking along the [001] direction. Besides, we find that the defect states, normally localized between V_{O2} and the neighboring Ti atom in the strain-free state, also readily break into two distinct orbital states in the O phase as illustrated in Figs. 4(b) and 4(c). The lower-level state is identical to the original $d_{x^2-y^2}$-dominant state, while the higher defect state is contributed by d_{xy}. Clearly the crystal symmetry breaking and the splitting of the $d_{x^2-y^2}$ orbit is responsible for the appearance of the new d_{xy} state.

As for the presence of V_{O3}, a similar situation is observed: a nonzero a spin moment is associated with the nonequivalent oxygen vacancy (V_{O3}) in the O phase, as well as in the triclinic phase when the misfit strain is larger than 3.0%. In the O case, magnetism is particularly distributed around the Ti atom adjacent to the O3 vacancy, similarly to the V_{O1}- and V_{O2}-induced spin moment. Strikingly, in the triclinic phase, the emerging spin moments with a positive or negative value are localized at two neighboring Ti atoms along the [010] direction [see Fig. 5(a)], leading to no net magnetic moment in the system. These results indicate that the interplay of oxygen vacancies and strain in the (110) epitaxial thin film can in fact bring about finite or locally canceled moments in $PbTiO_3$, depending on the V_i configuration. The nature of the locally canceled moments in V_{O3} is also present in the electronic defect states shown in Figs. 5(b) and 5(c). As in the case of the other oxygen vacancies, V_{O3}-induced spin-unpolarized impurity levels are symmetrically occupied by two electrons in the absence of a misfit strain. These impurity levels are formed from the dangling $d_{x^2-y^2}$-dominant orbital of two adjacent Ti atoms coordinating the vacancy site [see Figs. S2(e) and S2(f) in Supplemental Material Ref. [36]]. In contrast, V_{O3} in the O

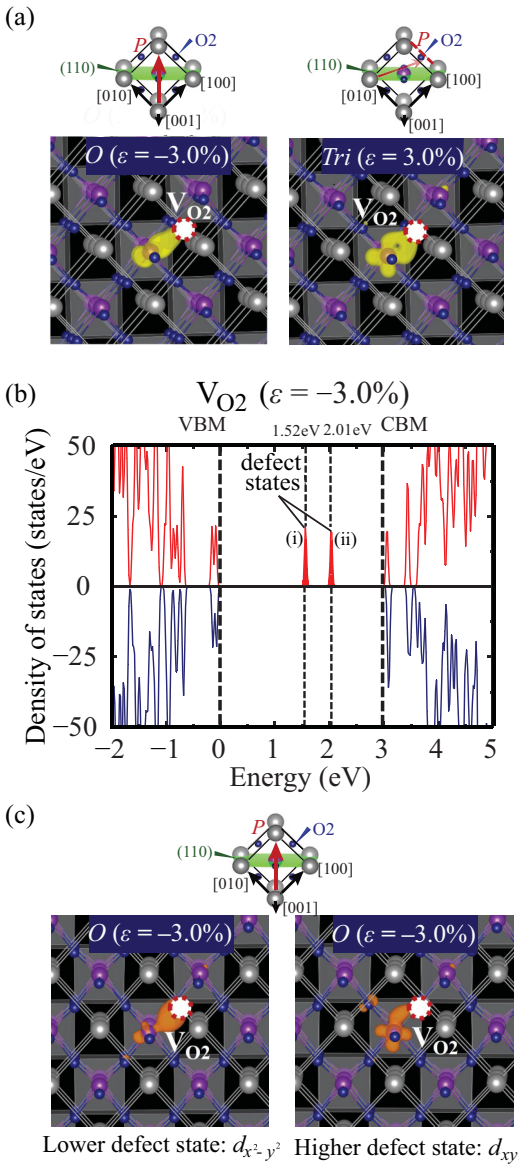

FIG. 4. (Color online) Spatial magnetization density distribution and defect electronic structures of V_{O2}. (a) Spatial magnetic spin-density distribution around V_{O2} in the triclinic and orthorhombic phases, respectively. (b) Electronic density of states (DOS) of magnetic V_{O2} in the orthorhombic phase. Red and blue indicate the majority and minority spin states, respectively. (c) Squared wave functions of the defect states in the orthorhombic phase. The original $d_{x^2-y^2}$ defect state break into lower-level $d_{x^2-y^2}$ and higher-level d_{xy} states in this phase. The orange and light blue iso-surfaces are the majority and minority spin densities of 0.015 $Å^{-3}$, respectively.

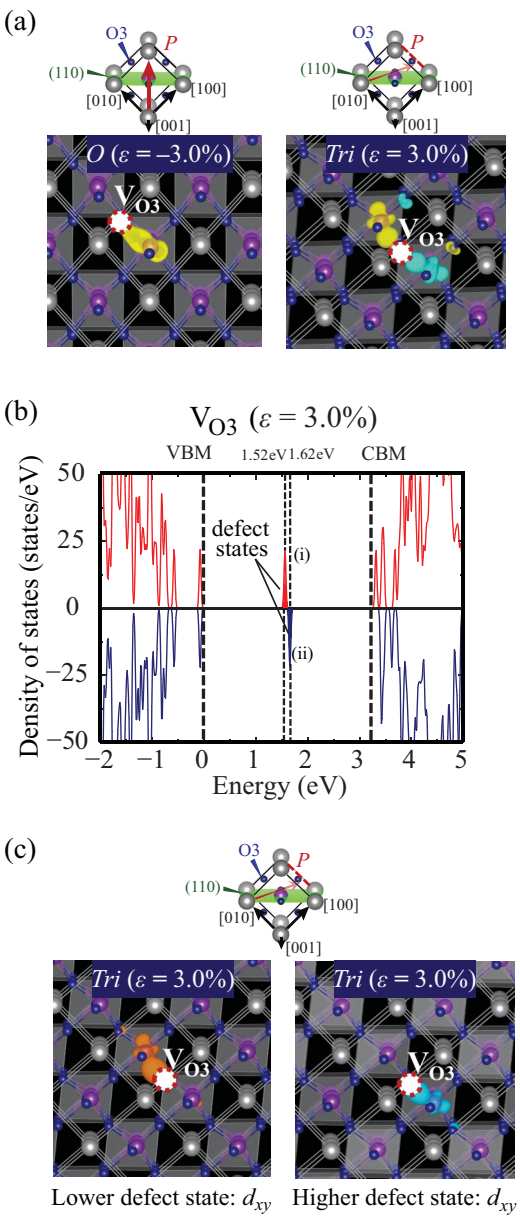

FIG. 5. (Color online) Spatial magnetization density distribution and defect electronic structures of V_{O3}. (a) Spatial magnetic spin-density distribution around V_{O2} in the triclinic and orthorhombic phases, respectively. (b) Electronic density of states (DOS) of magnetic V_{O3} in the triclinic phase. Red and blue indicate the majority and minority spin states, respectively. (c) The squared wave functions of the defect states in the orthorhombic phase. The original $d_{x^2-y^2}$ defect state break into up-spin d_{xy} and down-spin d_{xy} states. The orange and light blue iso-surfaces are the majority and minority spin densities of 0.015 $Å^{-3}$, respectively.

phase has in-gap states with two mixed $|\psi_e|^2$, mainly localized at the nearest Ti atom. The origin of the orbital splitting and the induced spin moment is similar to the symmetry breaking of V_{O2} in the O phase under compressive strain, so we will not go into it in detail here. However, we note that the electronic features of the defect are totally different in the triclinic phase under tensile misfit strain, where two defect states appear at slightly distinct energy levels of 1.52 and 1.62 eV above VBM, respectively, as illustrated in Fig. 5(b).

These two electronic-occupied states, mainly formed by d_{xy} states, have different spin directions: the lower defect state is up-spin, localized at the adjacent Ti atom, while the higher one is down-spin, localized at the other adjacent Ti atom [see Fig. 5(c)]. Upon comparing these two defect states with their strain-free counterpart, which is distributed purely along the [010] direction, it is natural to conclude that the split of the defect states may also be attributed to the [001] and

[010] symmetry break, as in the case of V_{O1} in the triclinic phase. It should be noted that this locally canceled moments may arise from the spin superexchange through indirect *d-d* hopping between the two equivalent Ti^{3+} ions paired by V_{O3}, as reported for oxygen vacancies in TiO_2 [37].

To assess the magnetic coupling between these moments, further calculations with two defects in the supercell are performed. We first consider two nearest-neighbor O1 vacancies separated by a distance of about 4.02 Å. The energy difference between the ferromagnetic and antiferromagnetic phases (interaction energy) is calculated to be 30 meV, indicating the stabilization of antiferromagnetic phase. We further increase the distance between the vacancies to about 7.01 Å and the antiferromagnetic phase is also found to be the ground state with its energy 10 meV lower than that of the ferromagnetic phase. Other interaction of the emerging local magnetic moments with different distances and strain states also turn out to be antiferromagnetic state according to calculations. Therefore, the coupling of the local magnetic moments in such a defect-strain system will induce a substantially long-range antiferromagnetic order.

C. Multiferroic phase transition and magnetoelectric coupling

We further demonstrate the (multi-)ferroic ground state and the marked influence of electric polarization on magnetism driven by oxygen vacancies, which are intrinsically and tightly coupled to each other. The misfit ferroic phase diagram of epitaxial (110) $PbTiO_3$ is shown in Fig. 6(a). The system remains purely ferroelectric (FE) without magnetism at zero misfit strain, owing to the unpolarized nature of all the oxygen vacancies. On the other hand, when the misfit strain increases to 0.5% or decreases to −1.8% magnetism turns to appear in the intrinsically ferroelectric phase, indicating the occurrence of a multiferroic phase transition under these misfit strains. Furthermore, the ME effect is evident: The initial [100] polarization can switch to the [010] direction by means of the applied electric field, leading to nonequivalent oxygen vacancy configurations, hence, the emergence of different magnetic characteristics. Figure 6(b) shows the magnetic phases of V_{O2} in the triclinic crystal phase ($\varepsilon = 3.0\%$) after switching of the polar axis and in the initial [100] polarization structure. Through this polarization switching, V_{O2} undergoes a rapid change of magnetic order (finite moment to locally canceled moments), which leads to the ME effect in epitaxial (110) $PbTiO_3$. The above results are observed because the V_{O2} in the [010] polarization state (after switching) is symmetrically identical to the V_{O3} in the initial [100] polarization system (before switching), which causes the V_{O2}- and V_{O3}-induced magnetic properties to interchange. Similarly, we can also get a phase transition of local magnetism to nonmagnetism and the resulting ME effect in the *O* phase through further polarization switching. When oxygen vacancies change their positions with the electric field, the ME coupling may be enhanced. For instance, when V_{O1} migrates to the V_{O2} site at $\varepsilon = -4.0\%$ by electric field, the magnetic moment emerges by this migration. However, the overall strength is not so much affected by such migration since decrease or enhancement of the ME coupling are both likely to occur based on different conditions. We should also remark that the oxygen vacancies only induce

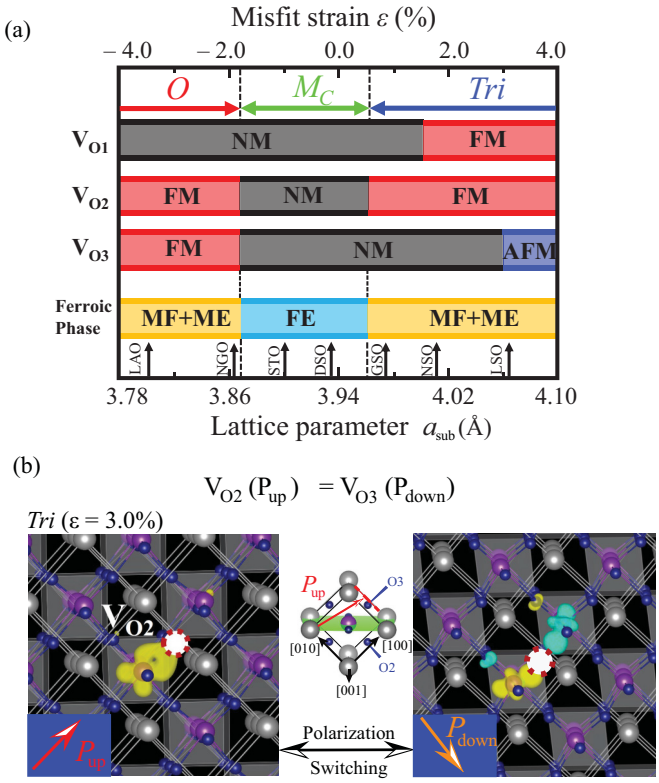

FIG. 6. (Color online) Multiferroic and magnetoelectric coupling in epitaxial (110) $PbTiO_3$. (a) Misfit ferroic phase diagram. Here FM denotes local magnetic order and AFM stands for magnetic moment in local antiferromagnetic arrangement. The lattice parameters for some candidate substrates, viz., $LaAlO_3$ (LAO), $NdGaO_3$ (NGO), $SrTiO_3$ (STO), $DyScO_3$ (DSO), $GdScO_3$ (GSO), $NdScO_3$ (NSO), and $LaScO_3$ (LSO), are also shown. (b) Magnetic phase transition of V_{O2} and V_{O3} via polarization switching in the triclinic phase.

slight ferroelectric disturbance locally and do not suppress the original ferroelectric at all according to our calculations, hence the expected magnetoelectric effect is attainable. Therefore, tuning of the unusual interaction between oxygen vacancies and mechanical strains with the appropriate choice of substrate provides an appealing route to realizing multiferroic transition and the magnetoelectric effect for conventional ferroelectrics.

IV. DISCUSSION

On the basis of the above results, here we suggest a new strategy for the synthesis of multiferroics by engineering the unusual defect-strain interaction. For perovskite oxides thin films, strains of several percent are common [38,39]. The epitaxial (110) $PbTiO_3$ considered here (from −4% to 4%) is experimentally feasible by commonly used practical substrates, such as $LaAlO_3$, $NdGaO_3$, $SrTiO_3$, $NdScO_3$, and $LaScO_3$ [16,40], and can completely sustain such a strain [41,42]. Note that the type and concentration of vacancies strongly depend on growth condition of materials: oxygen vacancies are prevailing and cation vacancies are hard to form under oxygen-poor condition, while Pb and Ti vacancies are likely to be formed under oxygen-rich conditions [14,43]. As a result, the formation of isolated oxygen vacancies,

rather than compensated by cation vacancies, in perovskite oxides is entirely favorable under oxygen-poor conditions, as has been widely confirmed by both direct experimental observation and theoretical studies [44,45]. Therefore, the situation presented here is experimentally feasible and thus realistic. In addition, the mobility of the oxygen vacancies can provide means of manipulation of MF and ME properties in terms of their concentration and distribution [46–50]. Thus, it becomes possible to spatially modulate the multiferroic order parameter through oxygen vacancy engineering, which leads to functional vacancies and even to a certain degree of control over the location, size, and distribution of oxygen vacancies [46,47]. The ability to manipulate the migration and diffusion of oxygen vacancies with an external electric field [48] or through other factors [49,50] also enables the multiferroic element to have a dynamic response. Such controllable variation of the multiferroic element is of interest from the viewpoint of potential application in future novel multiferroic memory devices.

Very recently it has been reported that dilute (anti-) ferromagnetism emerges in nanocrystals of ferroelectric $PbTiO_3$, whereas the origin was different from the present one, but was the grain boundaries coupled with oxygen vacancies [51–53]. Despite their different origins, the key for the unexpected ferromagnetism was also the defect states distinct from those in the bulk counterpart, which therefore support the present results for the similar mechanism. Thus, in addition to vacancy-grain boundary interactions, vacancy-strain interactions can also efficiently activate local magnetism in nonmagnetic ferroelectric materials and may enhance MF properties. We believe that the phenomena and mechanism we proposed here will lead to future awareness of magnetism in ferroelectrics and inspire further experimental study in this field. The basic design concept here can be transferred to other functional transition-metal oxides that are intrinsically nonmagnetic to induce magnetism, and has significant practical implications in the modification of material properties, which are usually governed by an interplay of several elementary processes.

V. CONCLUSION

In summary, we demonstrate the emergence of magnetism in oxygen-deficient (110) epitaxial ferroelectric lead titanate thin films and elucidate the electronic-level origin mechanism by performing hybrid Hartree-Fock density-functional calculations. The crystal phase transitions (Tri-M_C-O transitions) are determined as a function of the misfit strain. There is no magnetic spin polarization for oxygen vacancies in the strain-free state, while finite misfit strains induce spin moments with various magnetic configurations, depending on the symmetry breaking at the oxygen vacancy and the epitaxial strain conditions. The driven magnetic spin moment owes to spin-polarized defect states caused by orbital symmetry breaking due to crystal symmetry breaking through a misfit strain. In addition, the local magnetic phase at the defect can be electrically switched by reversing the polarization, which suggests nonlinear magnetoelectric coupling between magnetic and polarization orders. The present results provide a path towards the realization of multiferroics in conventional ferroelectrics, and will also provide significant insights into novel and extra functionalities in oxides.

ACKNOWLEDGMENTS

The authors acknowledge financial support for T.S. and T.K. through a Grant-in-Aid for Specially Promoted Research (Grant No. 25000012) and a Grant-in-Aid for Scientific Research (B) (Grant No. 26289006) from the Japan Society of the Promotion of Science (JSPS).

[1] W. Eerenstein, N. D. Mathur, and J. F. Scott, Nature (London) **442**, 759 (2006).
[2] S. W. Cheong and M. Mostovoy, Nat. Mater. **6**, 13 (2007).
[3] R. Ramesh, *Thin Film Ferroelectric Materials and Devices* (Kluwer Academic, Boston, 1997).
[4] J. F. Scott, *Ferroelectric Memories* (Springer, Berlin, 2000).
[5] N. A. Spaldin and M. Fiebig, Science **309**, 391 (2005).
[6] K. F. Wang, J.-M. Liu, and Z. F. Ren, Adv. Phys. **58**, 321 (2009).
[7] M. Fiebig, J. Phys. D **38**, R123 (2005).
[8] Y. Wang, J. Hu, Y. Lin, and C.-W. Nan, NPG Asia Mater. **2**, 61 (2010).
[9] B. Yin and S. Qu, Phys. Rev. B **89**, 014106 (2014).
[10] N. A. Hill, J. Phys. Chem. B **104**, 6694 (2000).
[11] C. L. Jia and K. Urban, Science **303**, 2001 (2004).
[12] O. N. Tufte and P. W. Chapman, Phys. Rev. **155**, 796 (1967).
[13] J. E. Garcia, V. Gomis, R. Perez, A. Albareda, and J. A. Eiras, Appl. Phys. Lett. **91**, 042902 (2007).
[14] T. Shimada, T. Ueda, J. Wang, and T. Kitamura, Phys. Rev. B **87**, 174111 (2013).
[15] Y. Umeno, T. Shimada, T. Kitamura, and C Elsasser, Phys. Rev. B **74**, 174111 (2006).
[16] D. G. Schlom *et al.*, Annu. Rev. Mater. Res. **37**, 589 (2007).
[17] T. Shimada, K. Arisue, J. Wang, and T. Kitamura, Phys. Rev. B **89**, 245437 (2014).
[18] O. Diéguez, K. M. Rabe, and D. Vanderbilt, Phys. Rev. B **72**, 144101 (2005).
[19] Q. Yang, J. X. Cao, Y. Ma, Y. C. Zhou, L. M. Jiang, and X. L. Zhong, J. Appl. Phys. **113**, 184110 (2013).
[20] D. J. Shu, S. T. Ge, M. Wang, and N. B. Ming, Phys. Rev. Lett. **101**, 116102 (2008).
[21] A. Grünebohm, M. Siewert, P. Entel, and C. Ederer, Ferroelectrics **429**, 1 (2012).
[22] J. Wang, T. Xu, T. Shimada, X. Wang, T. Y. Zhang, and T. Kitamura, Phys. Rev. B **89**, 144102 (2014).
[23] G. Kresse and J. Hafner, Phys. Rev. B **47**, 558 (1993).
[24] G. Kresse and J. Furthmüller, Phys. Rev. B **54**, 11169 (1996).
[25] P. E. Blöchl, Phys. Rev. B **50**, 17953 (1994).
[26] H. J. Monkhorst and J. D. Pack, Phys. Rev. B **13**, 5188 (1976).
[27] J. Heyd, G. E. Scuseria, and M. Ernzerhof, J. Chem. Phys. **118**, 8207 (2003).
[28] J. Heyd, G. E. Scuseria, and M. Ernzerhof, J. Chem. Phys. **124**, 219906 (2006).

[29] J. P. Perdew, K. Burke, and M. Ernzerhof, Phys. Rev. Lett. **77**, 3865 (1996).
[30] T. Shimada, T. Uratani, Y. Kitamura, and Takayuki, Appl. Phys. Lett. **100**, 162901 (2012).
[31] T. Shimada, Y. Uratani, and T. Kitamura, Acta Mater. **60**, 6322 (2012).
[32] F. Oba, A. Togo, I. Tanaka, J. Paier, and G. Kresse, Phys. Rev. B **77**, 245202 (2008).
[33] S. A. Mabud and A. M. Glazer, J. Appl. Crystallogr. **12**, 49 (1979).
[34] J. Robertson, W. L. Warren, and B. A. Tuttle, J. Appl. Phys. **77**, 3975 (1995).
[35] R. I. Eglitis, G. Borstel, E. Heifets, S. Piskunov, and E. Kotomin, J. Electroceram. **16**, 289 (2006).
[36] See Supplemental Material at http://link.aps.org/supplemental/10.1103/PhysRevB.92.104106 for magnetic diagrams in epitaxial (110) $PbTiO_3$ and defect electronic structures in strain-free $PbTiO_3$.
[37] K. Yang, Y. Dai, B. Huang, and Y. P. Feng, Phys. Rev. B **81**, 033202 (2010).
[38] S. Kumar, D. Kumar, V. G. Sathe, R. Kumar, and T. K. Sharma, J. Appl. Phys. **117**, 134103 (2015).
[39] D. G. Schlom, L.-Q. Chen, C. J. Fennie, V. Gopalan, D. A. Muller, X. Pan, R. Ramesh, and R. Uecker, MRS Bull. **39**, 118 (2014).
[40] N. Setter, D. Damjanovic, L. Eng, G. Fox, S. Gevorgian, S. Hong, A. Kingon, H. Kohlstedt, N. Y. Park, G. B. Stephenson, I. Stolitchnov, A. K. Taganstev, D. V. Taylor, T. Yamada, and S. Streiffer, J. Appl. Phys. **100**, 051606 (2006).
[41] S. B. Ren, C. J. Lu, H. M. Shen, and Y. N. Wang, Phys. Rev. B **55**, 3485 (1997).
[42] M. Ahart, M. Somayazulu, R. E. Cohen, P. Ganesh, P. Dera, H. K. Mao, R. J. Hemley, Y. Ren, P. Liermann, and Z. G. Wu, Nature (London) **451**, 545 (2008).
[43] S. K. Hau and K. H. Wong, Appl. Phys. Lett. **66**, 245 (1995).
[44] D. A. Muller, N. Nakagawa, A. Ohtomo, J. L. Grazul, and H. Y. Hwang, Nature (London) **430**, 657 (2004).
[45] S. Poykko and D. J. Chadi, Appl. Phys. Lett. **76**, 499 (2000).
[46] H. L. Tuller and S. R. Bishop, Annu. Rev. Mater. Res. **41**, 369 (2011).
[47] G. Y. Yang, G. D. Lian, E. C. Dickey, C. A. Randall, D. E. Barber, P. Pinceloup, M. A. Henderson, R. A. Hill, J. J. Beeson, and D. J. Skamser, J. Appl. Phys. **96**, 7500 (2004).
[48] S. J. Park *et al.*, Naotechnology **24**, 295202 (2013).
[49] G. L. Yuan, L. W. Martin, R. Ramesh, and A. Uedono, Appl. Phys. Lett. **95**, 012904 (2009).
[50] W. L. Warren, K. Vanheusden, D. Dimos, G. E. Pike, and B. A. Tuttle, J. Am. Ceram. Soc. **79**, 536 (1996).
[51] T. Shimada, J. Wang, T. Ueda, Y. Uratani, K. Arisue, M. Mrovec, C. Elsässer, and T. Kitamura, Nano Lett. **15**, 27 (2015).
[52] R. V. K. Mangalam, N. Ray, U. V. Waghmare, A. Sundaresan, and C. N. R. Rao, Solid State Commun. **149**, 1 (2009).
[53] M. Wang, G.-L. Tan, and Q. Zhang, J. Am. Ceram. Soc. **93**, 2151 (2010).